VOL. 12, NO. 10, MAY 2017 ISSN 1819-6608
ARPN Journal of Engineering and Applied Sciences


www.arpnjournals.com

DEVELOPMENT OF GAS-SENSITIVE LAYERS WITH NANOROD ARRAYS AND HIERARCHICAL NANOSTRUCTURES OF ZINC OXIDE

Ivanov V. V.[1], Tsepilov G. V.[1], Kazanov D. A.[2] and Voropai A. N.[1]
[1]CJSC, Technocomplekt, Shkol'naya St., Dubna, Moscow Oblast, Russia
[2]OOO, Turboenergoremont, Leninskii Prospect, Saint Petersburg, Leningradskaya Oblast, Russia
E-Mail: ivanov@techno-com.ru

ABSTRACT

In this paper the arrays of nanorods and hierarchical ZnO nanostructures were made suitable for large-scale production by electrochemical deposition method in a pulsed mode, which allows to control their morphology by varying deposition modes without changing the electrolyte composition. The crystal structure, morphology, optical and electrical properties of nanorod arrays and the hierarchical ZnO nanostructures were studied. The axial texture and the size of nanocrystallites in nanostructured ZnO arrays, their specific electrical resistivity, the height of Schottky grain boundary barriers, the concentration of uncompensated fully ionized donor impurity, the density of surface states at the grain boundaries and the width of the depletion region were determined. Gas sensitivity to low concentrations (10-200 ppmv) of ethanol vapor in air within the temperatures of 25-400 °C were demonstrated for nanorod arrays and hierarchical nanostructures of zinc oxide. According to the analysis of the structure and the properties of electrodeposited ZnO arrays in a pulse mode, the optimal regime was chosen for the manufacture and the operation of this material gas-sensitive layers in gas sensors.

Keywords: Impulse electrode position, gas sensitivity, structure, optical properties, AFM.

INTRODUCTION

Gas sensors based on metal oxides are the most widely used solid-state gas detection devices for domestic, medical, commercial and industrial purposes [1-15]. They have many advantages. Low cost and miniature sizes are among such advantages. However, the performance of such devices depends on the morphology and the structure of sensitive materials to a large extent. Thus, the achievement of high gas sensitivity for gas sensors based on single crystals of metal oxides or their dense films is a major problem. Therefore, the most promising trend is the development of nanostructured gas-sensitive layers on the basis of nanoporous or one-dimensional oxide-semiconductor arrays, and the hierarchical nanostructures of different forms are of special interest: coral-like, nanobrushes, nanocombs, dendrites and other things made from tin (SnO_2), titanium (TiO_2), zinc (ZnO), tungsten (WO_3), indium In_2O_3 oxides, etc. [1-9,11,13-14].

There is no single generally accepted idea about gas sensitivity mechanism of oxide-semiconductor gas sensors even now [1-2, 11]. It is assumed that the reaction to the gaseous medium is associated with the change in the electrical conductivity of the metal oxide due to the capture of electrons by adsorbed molecules and the induced variation of energy zone bending degree in a semiconductor caused by these charged molecules [1-2, 11]. As a rule, oxygen molecules from air or the molecules of another oxidizing gas are adsorbed on an oxide semiconductor surface and capture electrons, developing a negative charge at its trap centers and bending its energy zones upwards near the surface of nanocrystallites. Thus, a depleted layer is developed in the crystalline grains of a semiconductor, which reduces its electrical conductivity. When a sensor is exposed to reducing gases or, for example, ethanol vapors, the electrons from surface traps are returned to the volume of an oxide semiconductor crystalline grains, which leads to the potential barrier height decrease at the grain boundaries by the reduction of its energy zone bending and, consequently, to the conductivity increase of this semiconductor. According to [1], it is possible to distinguish three variants of gas interaction with a semiconductor on the basis of the relationship between the size of the semiconductor crystallites (D) and the width of the space charge layer (ω), which is developed in the near-surface layer of semiconductor grains due to gas chemisorption. According to [1], $\omega \approx 3$ nm in sintered porous SnO_2 layers. If $D >> 2\omega$, the material is not gas sensitive one, since the charge carriers inside the grains remain mobile irrespective of gas adsorption on the surface of grains. At $D \geq 2\omega$, the layers from the space charge regions form narrow conduction channels inside each crystallite. Consequently, the electrical conductivity depends not only on the height of the potential barriers at the boundaries, but also on the cross-sectional area of these channels, and therefore the particles with $D \geq 2\omega$ are sensitive to the surrounding gas composition. At $D<2\omega$, the space charge region dominates throughout the crystallite, which is almost completely depleted in terms of mobile charge carrier availability. In the case of $D <2\omega$, the energy semiconducting zones are almost flat ones across the entire interconnected grain structure, and there are no significant potential barriers at the grain boundaries, so electrical conductivity is controlled essentially by the grain boundaries. According to [1], a small number of charges acquired from surface reactions will cause significant conductivity changes of the entire structure, and thus, crystalline SnO_2 becomes particularly gas sensitive in the case when the size of its particles is less than 6 nm.

Such mechanism of gas sensitivity is described in [11] for ZnO. Recently ZnO nanostructures are considered to be the most promising material for the production of highly sensitive and selective gas sensors [8, 11-16]. Zinc oxide is a nontoxic and an inexpensive semiconductor with a prohibited zone width of ≈3.37 eV, with the dominant defects in the form of oxygen vacancies VO [2,7-9,13-16], has a high mechanical and chemical stability. It is recommended to use various ZnO nanostructures in gas sensors, such as nanorods, nanowires, nano-micro-flowers, quantum dots, thin films, nanotapes, nanodiscs, nanosheets, etc. In order to determine the concentration of nitrogen dioxide (NO_2) [11], ethanol (CH3-CH2-OH) [12,14], acetone (CH3-C(O)-CH3) [13], hydrogen (H2) [16] and other gases and vapors. A considerable surface-to-volume ratio in ZnO hierarchical nanostructures with one-dimensional or two-dimensional nanostructures as their building blocks makes them particularly promising for high-performance gas sensors [8, 13-16]. The authors of [16] point to the need of a careful control concerning the geometry of ZnO nanostructures, since they observed the loss of gas sensitivity to hydrogen in the thinnest nanowires due to the appearance of "flat zone state" for this material (in contrast to SnO_2) in the case when ω reaches half of ZnO diameter. In [17], during the process of electrical properties modeling in respect of polycrystalline ceramic semiconductors with submicrometer crystal grains (coherent scattering regions) D and during the study of Schottky double barriers at grain boundaries, it was also found that at 2ω ≥ · D the polycrystalline material is in "the state of flat zones". In other words, it behaves like a homogeneous dielectric due to the overlapping of adjacent Schottky double barriers. According to [17], as the value of D increases, the specific capacitance of nanostructures increases with the constant value ω due to the formation of discrete double Schottky barriers in a grain boundary region. With the further enlargement of grains, C decreases due to the reduction of grain boundaries number. Thus, by analyzing the capacitive characteristics of zinc oxide nanostructures, it is possible to assess their potential suitability for the use in gas sensors.

Based on the mentioned above, the data about the structure and the electrical properties of this material, in particular about the size of the nanocrystallites D, the electric resistivity p, the height of Schottky barrier, φ, the concentration of the uncompensated completely ionized donor impurity Nd, the density of the surface states at grain boundaries N_{ss} and the width of the depletion region ω are important for the creation of gas-sensitive ZnO nano arrays. In this paper the arrays of nanorods and hierarchical ZnO nanostructures were made suitable for large-scale production by electrochemical deposition in a pulsed mode, which allows to control their morphology by varying the deposition regimes in the same galvanic bath without the electrolyte composition change. The crystal structure, morphology, optical and electrical properties of nanorod arrays and hierarchical ZnO nanostructures were studied. On the basis of structure analysis and electrodeposited ZnO array properties in pulse mode an optimum mode of their production was selected. They demonstrated gas sensitivity in respect of small concentrations (10-200 ppmv of ethanol vapor in air at the temperatures of 25-400 °C for nanorod arrays and hierarchical nanostructures of zinc oxide.

Experiment procedure

The production of zinc oxide arrays was performed by pulsed electrochemical deposition in a three-electrode electrochemical cell with an unmixable aqueous electrolyte containing 0.05 M of $Zn(NO_3)_2$ and 0.1 M of $NaNO_3$. They used glass plates coated with transparent conductive layers of fluorine doped tin oxide (SnO_2: F, or FTO) from Pilkington company, USA as substrates (cathodes or working electrodes). Platinum helix was used as a counterelectrode, and a saturated chlorine-silver Ag/AgCl electrode was used as a reference electrode. Using a pulsed potentiostat equipped with a programmer the rectangular potential pulses were sent to the cathode substrate to perform pulsed electrolysis, so that the lower limit of the cathode potential relative to the reference electrode U_{off} was -0.8 V and the upper limit of U_{on} was -1.4 V (potentials are presented relative to the reference electrode Ag/AgCl). Thus, the amplitude of the cathode potential change was 0.6 V during pulsed electrolysis. The duty cycle (Dc = 0.4) was calculated by the following formula:

$$Dc = \frac{T_{on}}{(T_{on} + T_{off})} = T_{on} \cdot f \quad (1)$$

Where T_{on} is the time during the cathode potential U_{on}; T_{off} is the time during the cathode potential U_{off}; F is the frequency, that is, the value reciprocal of the cycle time T_c:

$$f = \frac{1}{(T_{on} + T_{off})} = \frac{1}{T_c} \quad (2)$$

During the electric deposition of each individual sample from the array of nanorods or ZnO hierarchical nanostructures for 1 hour, the pulse frequency f was kept constant at f = 2 Hz. If the temperature remained unchanged during the entire electrode position process and was 70 °C, we obtained the arrays of nanorods ZnO shown on Figure-1 (a) The hierarchical nanostructures shown on Figure-1 (b) in the form of small nanorods or the branches of zinc oxide on the surface of large ZnO nanorods were developed by electrolyte cooling during the sample electrode position from 85 °C to 70 °C.

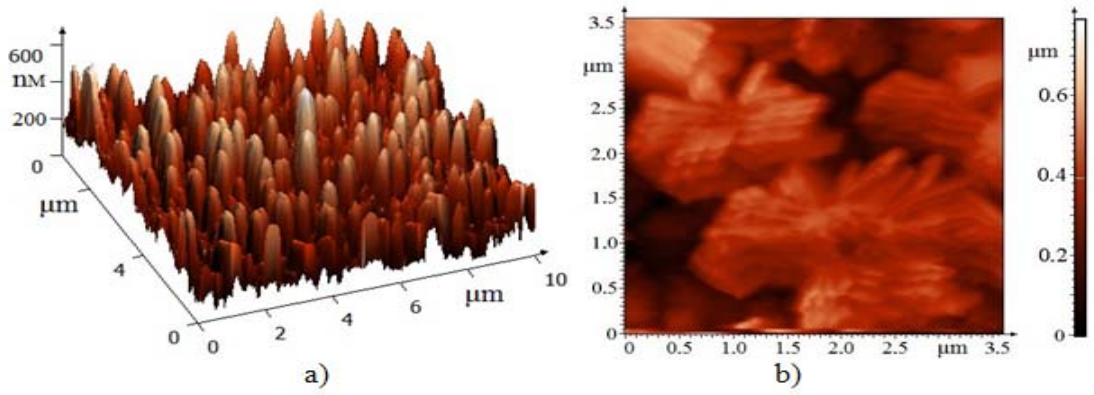

Figure-1. AFM image of ZnO arrays (a) and hierarchical nanostructures of ZnO (b) made by pulsed electrodeposition.

The study of zinc oxide array optical properties was carried out in the spectral range of 350-850 nm using a SF-2000 spectrophotometer equipped with a mirror and diffuse reflection attachment SFO-2000. They used the substrates of FTO/glass from Pilkington company, USA as the control samples during the record of optical transmittance coefficient spectrum T(λ). The optical width of the restricted zone E_g for zinc oxide layers was determined by the extrapolation on the axis of linear dependence section $[-\ln(T)\cdot h\nu]^2$ from hν. The light scattering factor (Hf, Haze factor) was calculated as the ratio of diffuse reflection to the total reflection R (the sum of diffuse and mirror reflections).

In order to analyze the structural and sub-structural parameters of ZnO arrays, the X-ray spectra were recorded using DRON-4 diffractometer in CoKα radiation (λCoKα = 1.7889 Å). The scanning was performed with Bragg-Brentano focusing (θ-2θ). The processing of obtained X-ray diffractograms (separation of background, separation of the doublet Kα1-Kα2, etc.) as well as calculation of the diffraction line profile parameters was carried out using the programs "New_Profile v.3.4 (486)" and "OriginPro v.7.5". The presence of crystalline phases was detected by comparing the data of experimental X-ray diffraction patterns with the reference data base JCPDS using the program "PCPDFWIN v.1.30". The estimation of coherent-scattering domain (D) size, which is usually also considered as the size of nanocrystallites or ZnO grains [10], and the values of microstresses Δd/d (where d is the crystal lattice period according to JCPDS, Δd is the difference between the experimental and the reference values of the crystal lattice period) in zinc oxide arrays were performed by the analysis of X-ray diffraction maxima broadening, taking into account the presence of instrumental broadening by Williamson-Hall approximation method. The crystal lattice parameters a and c of zinc oxide hexagonal phase were calculated from the position of two last indexed x-ray diffractograms by Nelson-Rilli graphical extrapolation method (NRM) and were cleared by the least squares method (LSM) using the "UnitCell" program and all recorded X-ray diffraction patterns. The residual stresses σ in zinc oxide arrays were calculated on the basis of data about the lattice periods of electrodeposited c and the reference samples c_{bulk} using the values of material elasticity constants in different directions:

$$\sigma = -233 \cdot \frac{c - c_{bulk}}{c_{bulk}}; \quad c_{bulk} = 5,206 \tag{3}$$

In order to determine the axial texture of electrodeposited zinc oxide arrays according to Harris method they used the values of x-ray diffractometric peak integrated intensities. For each peak they calculated the value of the pole density P_{hkl}, which characterizes the probability with which the normal to the nanocrystallite surface coincides with the normal to the plane (hkl), i.e. determines the number of nanocrystallites which have (hkl) planes parallel to the sample surface. The pole densities were calculated for all recorded x-ray diffractometric peaks, the values of $P_{hkl} >> 1$ were assigned to the texture axes.

The study of zinc oxide array morphology was performed by a semi-contact method of atomic power microscopy (APM) using the device "NanoLaboratory Integra Prima NT-MDT".

In order to study the electrical and electronic parameters of the deposited electrodes on FTO nanorod array substrates and the hierarchical nanostructures of zinc oxide, metal contacts were made of aluminum. Aluminum was chosen as a contact material, because, due to the ratio of Al output operation (W_{Al} = 4.06-4.26 eV) and the electron affinity of ZnO (χZnO = 4.2 eV), it provides the formation of ohmic contacts with zinc oxide according to [18-19]. In order to avoid shunting, the vacuum deposition of Al was carried out at the angle of 75º to substrates with ZnO layers on their limited zones with the area of Sc (from $2\cdot10^{-2}$ to $7.5\cdot10^{-2}$ cm^2) through a shadow mask made of aluminum. Then electrically conductive glue with silver filler "Kontaktol" was applied to the surface of aluminum metallization. This glue provided the galvanic contact with the metallization of flexible outputs in the form of copper microwires. Such 2-nd series of Al/FTO/ZnO/Al test samples (one with the arrays of ZnO nanorods and the other one with the arrays of hierarchical ZnO

nanostructures), which are schematically depicted on Figure-2, were used to measure volt-ampere characteristics (VAC) and volt-farad characteristics (VFC) of nanorod arrays and hierarchical ZnO nanostructures, as well as to study their gas sensitivity with respect to ethanol.

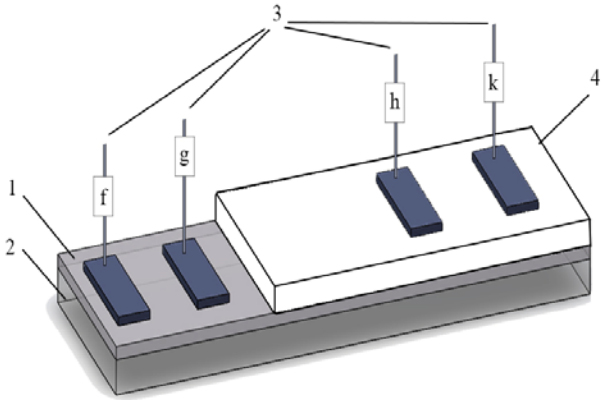

Figure-2. - Schematic representation of Al/FTO/ZnO/Al test sample to measure the gas sensitivity of arrays from nanorods or hierarchical ZnO nanostructures with respect to ethanol: 1 - FTO; 2 - glass; 3 - contacts from Al with "Kontaktol" glued copper microwire; 4-ZnO.

The volt-ampere characteristics were recorded by characteristic tracer method [19] when Al/FTO/ZnO/Al test samples were connected to the "L2-56 semiconductor device parameter meter", which provides the visualization of the VAC on its screen. The polarity of bias voltage U corresponded to the negative potential at FTO and the positive one on ZnO. From the VAC measured in the case of both aluminum contacts arrangement on the surface of FTO layer, the impedance value of this layer was obtained Rt = U/I, after which the specific resistivity ρFTO of the transparent conductive layer FTO was calculated by the following formula:

$$\rho_{FTO} = R_t \cdot S_{FTO}/w, \quad (4)$$

where S_{FTO} is the product of the aluminum contact length and the thickness of FTO layer; w is the slit width between two parallel banded aluminum contacts located on FTO top. The value of ρ FTO = 3.5×10^{-4} Ωxcm obtained by us with VAC corresponds to the certificate data for FTO of TEC 7 brand from Pilkington company, USA. The calculation of hierarchical zinc oxide nanostructures ρ specific resistivity based on the results of VAC measurement in the region of its ohmicity when aluminum contacts are placed on zinc oxide array surface and on FTO was performed according to the following formula:

$$\rho = (U/I - \rho_{FTO} \cdot L/S_{FTO}) \cdot S_c/(\zeta \cdot t) \quad (5)$$

where U is the voltage corresponding to the ohmic section of VAC; I is the current corresponding to this voltage; L is the distance between parallel band contact electrodes of equal area Sc on the surface of zinc oxide arrays and on FTO; t is the average length of ZnO nanorods or the total length of the connecting Al and FTO branches of ZnO hierarchical nanostructures (t ≈ 1.10 μm); ζ is the coefficient that takes into account the total area of voids in the arrays of nanorods and hierarchical nanostructures ZnO (ζ > 1).

If both parallel striped contacts from Al were located on the surface of nanorods and hierarchical nanostructures ZnO, then the following relation was used to calculate ρ along the ohmic section of the measured VAC:

$$\rho = (U/I - \rho_{FTO} \cdot l/S_{FTO}) \cdot S_c/(2 \cdot \zeta \cdot t), \quad (6)$$

where l is the distance between the centers of parallel banded contact electrodes of equal area.

The measurement and the analysis of FVC arrays of nanorods and ZnO hierarchical nanostructures were performed for the same Al/FTO/ZnO/Al test samples, which were studied by VAC method. In order to measure FVC they used "L, C, R digital meter E7-12" at the frequency of 1 MHz and the measuring voltage amplitude of 0.03 V. The value of the constant bias voltage U applied to the test sample from the internal source in forward or reverse direction was regulated within the values of $0 \le |U| \le 1.5$ V. Specific capacitance C values for hierarchical nanostructures ZnO were obtained by the measured capacitance division into the area of S_c/ζ aluminum metallization contact with the arrays of ZnO nanostructures. In order to perform FVC analysis they applied the technique used in [17, 21-22] during the description of electrical properties and electronic parameters of polycrystalline semiconductors and varistors based on ZnO. This technique is based on the model of double symmetric Schottky barrier appearance with φ height in grain boundary ZnO areas.

According to [21-22], the concentration of uncompensated ionized donor impurity Nd in ZnO grains and the barrier height φ at the grain boundary were determined from the tangent of rectilinear segment slope angle to the bias voltage U axis and the intersection point with the U axis of this segment extension on the dependence graph $(1/C - 1/(2 \cdot C_0))^2$ from U, which is described by the following formula:

$$(1/C - 1/(2 \cdot C_0))^2 = 2 \cdot p^2 \cdot (\varphi + U/p)/(q \cdot \varepsilon_0 \cdot \varepsilon \cdot N_d), \quad (7)$$

where C_0 is the specific capacity of the grain boundary at the voltage $U = 0$; q is the electron charge, ε_0 is the electric constant, $\varepsilon \approx 8.5$ is the relative dielectric permittivity of zinc oxide, $p = t/D$ - the number of barriers between the grains along the length of ZnO nanorod, or along the total length of the connecting FTO and Al branches of ZnO hierarchical nanostructures. The density

of states at N_{SS} grain boundary and the width of the layer w depleted by mobile charge carriers on both sides of the grain boundary were calculated using the following relations:

$$N_{SS} = (2 \cdot \varepsilon_0 \cdot \varepsilon \cdot N_d \cdot \varphi / q)^{1/2}, \quad (8)$$

$$\omega = N_{SS}/N_d. \quad (9)$$

The gas sensitivity of nanorod arrays or ZnO hierarchical nanostructures with respect to ethanol was measured using the same Al/FTO/ZnO/Al test samples at the temperatures within the range of 25-400 ºC. To do this, the test sample was loaded into a quartz reactor placed into a tube furnace, where a certain concentration (in the range of 10-200 ppm^{-1}) of ethanol vapor in air was fed. The gas sensitivity of nanorod arrays or ZnO hierarchical nanostructures to ethanol vapors S was determined in accordance with [7,10] as the ratio of electrical currents flowing through the Al/FTO/ZnO/Al test sample with ethanol vapors (Ie) in air and in clean air (Iв) at the same bias voltage U = 1 V, that is, according to the formula S = Ie/Iв. After each measurement, the quartz reactor was purged with clean air. The response time was noted as a necessary one to achieve 63% of the maximum current Ie passing through the test sample at a bias voltage U = 1 V after the introduction of ethanol vapors into the reactor. The decay time of the signal was determined as a necessary one to achieve 37% of Ie after the reactor purging with clean air. The reproducibility and the stability of Al/FTO/ZnO/Al test samples as the basis of oxide-semiconductor-type gas sensors was tested by conducting a series of experiments on the introduction and the removal of ethanol vapors in the range of its concentrations 10-200 ppm^{-1} at the temperatures of 25-400 °C.

RESULTS AND DISCUSSION

Figure-3 shows the images of nanostructured arrays obtained by atomic power microscopy that were produced in the above described modes by pulsed electrodeposition method. It can be seen that the ZnO nanorods with the diameter of 200-400 nm on Figure-3a have a smooth surface, while the hierarchical nanostructures on Figure-3b are low ZnO nanorods with the diameter ≈ 400 nm perpendiculars to which the finer branches of this material with the diameters ≈ 100 nm diverge in different directions. It is obvious that at the same length of nanorods and the sum of the thick and the thin branch lengths in the hierarchical nanostructure, the surface area of hierarchical nanostructure array exceeds the array area of ZnO nanorods many times.

Figure-3 shows the X-ray diffraction patterns of nanostructured ZnO arrays of both types, that is, the nanorods and hierarchical nanostructures, and Table-1 shows the results of these arrays structural and sub-structural parameters calculation. X-ray diffractograms show that both arrays are nanocrystalline and single-phase ones, have hexagonal ZnO structure of wurtzite modification (JCPDS 36-1451), are characterized by increased parameters of crystal lattices along c axis as compared to the reference ZnO (according to JCPDS 36-1451, a = 3.250 Å, c = 5.207 Å), as well as insignificant microstresses Δd/d and residual stresses of σ compression. The comparison of the coherent scattering regions D presented in Table-1 shows a substantially larger nanocrystallite size for ZnO nanorods as compared to the hierarchical nanostructures of this material. The analysis of the axial texture of a ZnO nanorod array shows a pronounced texture in the perpendicular direction relative to the substrate (P_{002} = 3.44), which is typical for such nanostructures [11, 16]. At the same time, the hierarchical nanostructure is practically not textured one, it agrees well with [11] and with the morphology of its surface shown on Figure-3b.

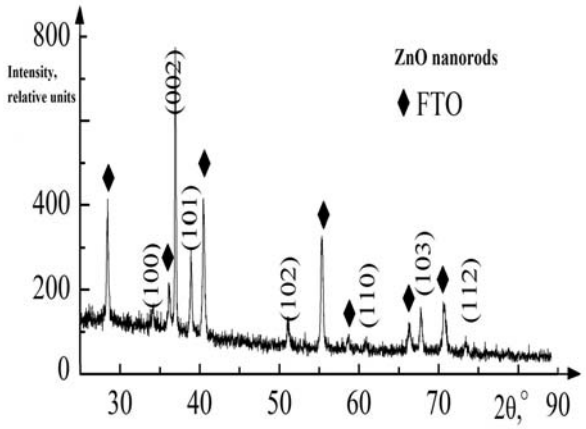

(a)

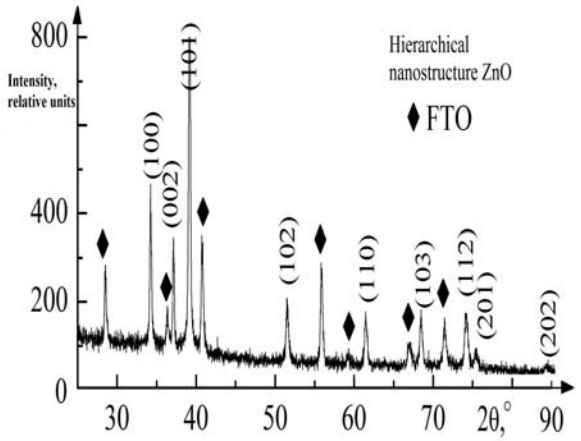

(b)

Figure-3. X-ray diffraction patterns of ZnO nanostructured nanorod arrays (a) and (b) ZnO hierarchical nanostructures ($Co_{K\alpha}$ radiation) electrodeposited into FTO substrates.

Table-1. Structural and sub-structural parameters of nanorod arrays and the hierarchical nanostructures of zinc oxide.

ZnO array	*D*, nm	$\Delta d/d \cdot 10^3$	σ, GPa	Lattice parameters, Å				Texture	
				Nelson-Rilly method		Least square method		Pole density, P_{hkl}	*h k l*
				a	c	a	c		
Nanorods	70 – 190	0,8-1,6	-0,54	3,256	5,217	3,256	5,218	3,44	(002)
Hierarchical nanostructures	40 – 90	0,4-1,3	-0,54	3,249	5,221	3,251	5,218	1,70 1,56 1,40 1,04	(112) (101) (102) (100)

According to Figure-4 the optical properties of two types of nanostructured zinc oxide arrays were differed mainly by the lower transparency of hierarchical nanostructures (T(λ) spectra on Figure-4a and their more significant reflection and light scattering (R(λ) and Hf(λ) spectra on Figure-4c). The determination of the prohibited zone Eg optical width using the graphical dependences shown on Figure-4b demonstrated that the material of nanostructured arrays is wide zoned one (Eg = 3.1 - 3.2 eV), its Eg is by 0.1 - 0.2 eV smaller than that of single-crystal ZnO.

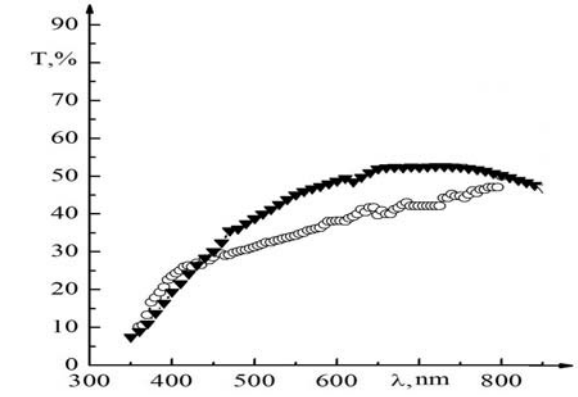

(a)

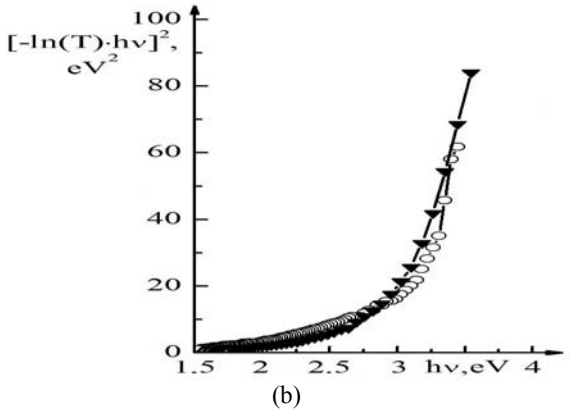

(b)

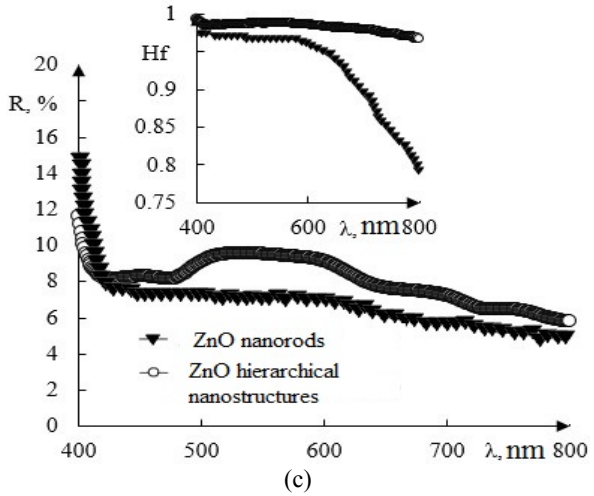

(c)

Figure-4. The optical properties of electrodeposited nanostructured arrays of ZnO nanorods and ZnO hierarchical nanostructures in a pulsed mode: optical transmission coefficient spectra T(λ)(a); The dependence of $[(-\ln T)\cdot h\nu]^2$ on the energy of quanta to determine the width of the forbidden zone for direct optical transitions in ZnO (б); Reflection spectra R(λ) (в); Insertion in (в) - light scattering factor Hf(λ) spectra.

The results of the study presented on Figure-5a concerning the dependence of the specific resistivity ρ of nanostructured ZnO arrays on their grain size D showed that regardless of nanostructured zinc oxide arrays development by nanorods or hierarchical nanostructures, their resistance decreases as nanocrystallites increase. As can be seen on Figure-5b, the dependence of the specific capacitance at zero bias Co from D has the form of a curve with a maximum and is also virtually unrelated to the morphology of nanostructured ZnO arrays for these arrays. The graph for Co as D function (Figure-5b) has the maximum at the sizes of ZnO coherent scattering regions in the range 70-85 nm. Thus, the formation of Schottky double barriers in the grain boundary region described in [17] for ZnO arrays electrodeposited in pulsed mode is observed in the grain boundary region, including the

overlapping of adjacent Schottky double barriers at D < 70 nm and capacity decrease due to enlargement of ZnO grains at D > 85 nm. Based on VAC measurement results and the calculations performed using the graphical dependences shown on Figure-5c, the electronic and electrical parameters of electrodeposited nanorod arrays in pulsed mode and hierarchical ZnO nanostructures were determined and presented in Table-2. The analysis of these parameters confirms that during the enlargement of coherent scattering regions in nanostructured arrays of zinc oxide the concentration of the uncompensated ionized donor impurity Nd increases from 1.6×10^{16} (hierarchical ZnO nanostructures) to 5.6×10^{17} cm^{-3} (ZnO nanorods). According to [18, 23], the values of Nd ~ 10^{16} cm^{-3} are the typical ones for a nominally undoped ZnO with a specific n-type of conductivity, caused by small donor defects in the form of oxygen vacancies and interstitial zinc. An increase from D of Nd values is accompanied by the increase of double Schottky barrier height on the boundaries of the coherent scattering regions and the decrease of the depletion region ω width. The array of ZnO nanorods with relatively large dimensions D (in the range of 70-190 nm) demonstrates narrower depletion regions (ω ≈ 38 nm). The condition ω ≤ 1/2·D is fulfilled, therefore the material has high double Schottky barriers on the boundaries of coherent scattering regions (W ≈ 0.84 eV), which agrees well with its minimum resistance ρ (Figure-5 a) and with the highest Nd value (Table-2). The array of hierarchical ZnO nanostructures with the dimensions of coherent scattering regions D in the range of 40-90 nm, the width of the depletion region ω = 97 nm conditioned by Schottky barriers at their boundaries exceeds the size D. Therefore, the barriers are small (φ ≈ 0.17 eV). As can be seen from Table-2, both types of ZnO nanostructures are characterized by a high density of NSS surface states from $1.6 \cdot 10^{11}$ to $2.1 \cdot 10^{12}$ cm^{-2}, which confirms a significant disorientation of the coherent scattering regions. At the same time, in accordance with [1, 11, 17], in the aggregate of electrical and electronic parameters, the hierarchical nanostructures of zinc oxide should have a higher gas sensitivity than the arrays of ZnO nanorods.

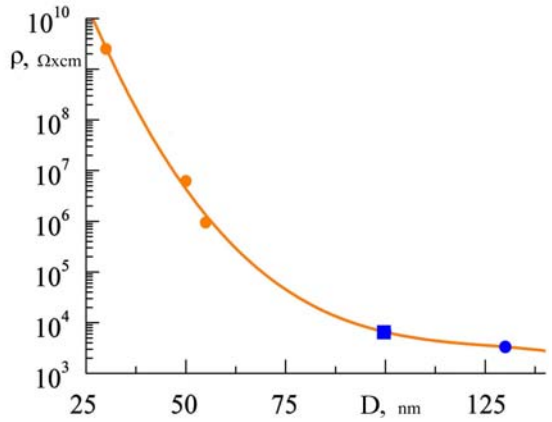

(a)

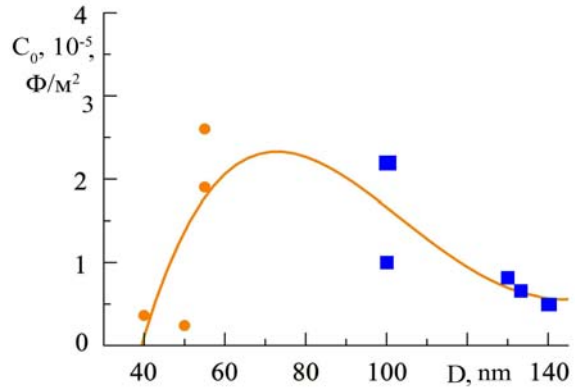

(b)

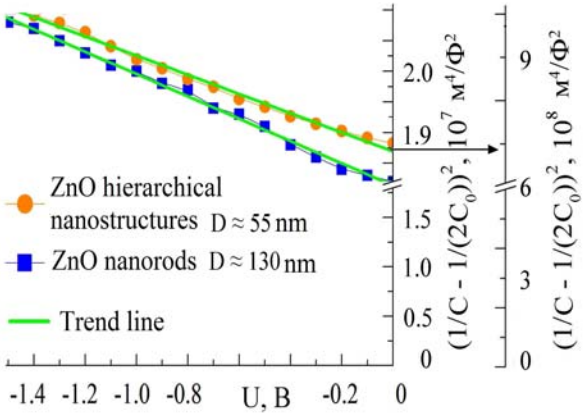

(c)

Figure-5. The graphs for the determination of electronic and electrical parameters electrodeposited in a pulsed mode of nanorod arrays and hierarchical nanostructures ZnO: a - specific resistivity ρ dependence on grain size D of nanostructured ZnO arrays; б - the specific capacitance dependence on D at zero bias Co; в - dependences for electronic parameters of ZnO nanostructures calculation in accordance with [16-17,22].

Experimental studies showed that the hierarchical ZnO nanostructures have the gas sensitivity greater by an order approximately than the arrays of nanorods from this material. As can be seen from the experimental dependencies of nanorod array gas sensitivity and the hierarchical nanostructures on the temperature (Fig. 6a), the optimum temperature for ethanol vapor record in air by both nanostructured ZnO arrays is 220 °C. Figure. 6b shows that within the following concentration range of ethanol in air 40 - 200 ppmv, the gas sensitivity dependence on the ethanol concentration is a linear one. Through the series of experiments on the introduction and removal of ethanol vapors within the range of its concentrations 10-200 ppmv at the temperatures of 25-400 °C, it was possible to demonstrate the reproducibility and the stability of Al/FTO/ZnO/Al test sample operation.

Table-2. Electronic and electrical parameters of electrodeposited nanostructured ZnO arrays in pulsed mode.

ZnO array	D, nm	φ, V	p	N_d, cm^{-3}	N_{SS}, cm^{-2}	ω, nm
Nanorods	70 – 190	0.84	9	$5.6 \cdot 10^{17}$	$2.1 \cdot 10^{12}$	38
Hierarchical nanostructures	40 – 90	0.17	20	$1.6 \cdot 10^{16}$	$1.6 \cdot 10^{11}$	97

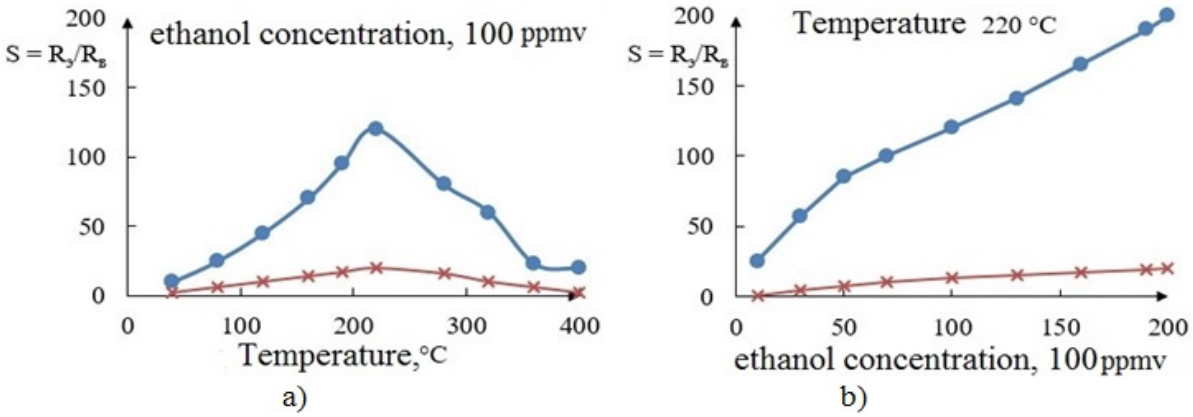

Figure-6. The dependence of Al/FTO/ZnO/Al test sample gas sensitivity with the arrays of nanorods and ZnO hierarchical nanostructures on the temperature at the concentration of ethanol vapors in air of 100 ppmv (a) and on the concentration of ethanol vapor in air at 220 °C (b).

Figure-7 shows the response curves on ethanol feeding into the reactor and on the removing of ethanol from the air for nanorod arrays and hierarchical nanostructures of zinc oxide. The comparison of response curve shape allows us to conclude that the test samples of Al/FTO/ZnO/Al with the arrays of hierarchical nanostructures have ~ 2 times shorter response period and signal attenuation period as compared to ZnO nanorods, which is the characteristic of gas sensor increased speed that will be created on the basis of hierarchical ZnO nanostructures.

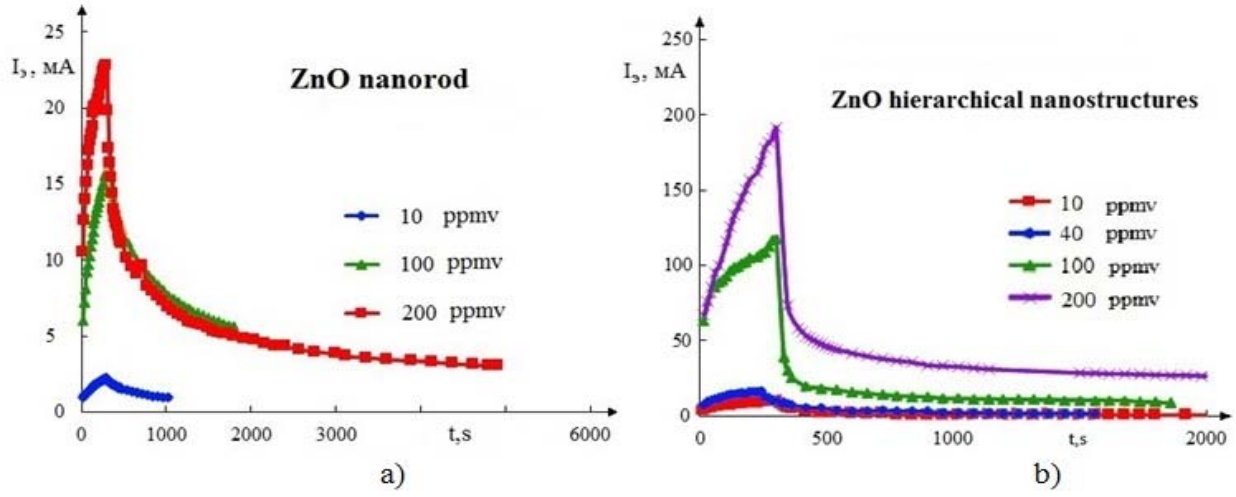

Figure-7. The response curves for the presence of various concentrations of ethanol vapors in air obtained at the temperature of 220 °C for ZnO nanorod arrays (a) and ZnO hierarchical nanostructures (b).

CONCLUSIONS

Based on the results of morphology, crystal structure, optical and electrical properties study, it was revealed that the method of pulsed electrochemical deposition allows to produce the arrays of not only ZnO nanorods but also of this material hierarchical nanostructures, and, in combination of characteristics the hierarchical nanostructures are more promising for the use as the basis for the gas sensors of oxide-semiconductor type. Stable high gas sensitivity was demonstrated at the temperature of 220 °C among Al/FTO/ZnO/Al test samples with the arrays of hierarchical ZnO nanostructures with respect to ethanol vapors. The ethanol concentration in the air from 40 to 200 ppmv provides a linear dependence of gas sensitivity on the concentration of ethanol.

ACKNOWLEDGEMENTS

This article was prepared as a part of the implementation of applied research and experimental development (ARED) on the Agreement on the subvention (2015, October, 27) No. 14.579.21.0113 with the financial support of the Ministry of education and science of the Russian Federation. A unique identifier of ARED - RFMEFI57915X0113.

REFERENCES

[1] Sun Y.-F., Liu S.-B., Meng F.-L., Liu J.-Y., Jin Z., Kong L.-T.,. Liu J.-H.. Metal oxide nanostructures and their gas sensing properties: a review // Sensors. 2012. V. 12. P. 2610–2631.

[2] Neri G. First fifty years of chemoresistive gas sensors // Chemosensors. 2015. V. 3. P. 1-20.

[3] Huang J., Wan Q. Gas sensors based on semiconducting metal oxide one-dimensional nanostructures // Sensors. 2009. V. 9. P. 9903–9924.

[4] Obvintseva L.A. Semiconductor metal oxide sensors to determine chemically active gas impurities in the air, Rus. Chem. Jor. (The Journal of Russian Chemical Society named after D.I. Mendeleyev). 2008. V. LII, No. 2. pp. 113-121.

[5] Ramgir N.S. Electronic nose based on nanomaterials: issues, challenges, and prospects // ISRN Nanomaterials. 2013. V. 2013. Article ID 941581, 21 pages.

[6] Yamazoe N. Toward innovations of gas sensor technology // Sensors and Actuators. 2005. V. B 108. P. 2–14.

[7] Ahn M.-W., Park K.-S., Heo J.-H., Park J.-G., Kim D.-W., Choi K.J., Lee J.-H., Hong S.-H. Gas sensing properties of defect-controlled ZnO- nanowire gas sensor // Applied Physics Letters. 2008. V. 93. P. 263103-1–263103-3.

[8] Pan X., Liu X., Bermak A., Fan Z. Self-gating effect induced large performance improvement of ZnO nanocomb gas sensors // ACS Nano. 2013. V. *7*(10). P. 9318–9324.

[9] Peng S., Wu G., Song W., Wang Q. Application of flower-like ZnO nanorods gas sensor detecting SF_6 decomposition products // Journal of Nanomaterials. 2013. V. 2013, Article ID 135147, 7 pages.

[10] Hjiri M., El Mir L., Leonardi S.G., Donato N., Neri G. CO and NO_2 selective monitoring by ZnO-based sensors // Nanomaterials. 2013. V. 3. P. 357-369.

[11] Kumar R., Al-Dossary O., Kumar G., Umar A. Zinc Oxide Nanostructures for NO_2 Gas–Sensor Applications: A Review // Nano-Micro Letters. 2015. V. 7(2). P. 97–120.

[12] Wang L., Kang Y., Liu X., Zhang S., Huang W., Wang S. ZnO nanorod gas sensor for ethanol detection // Sensors and Actuators B. 2012. V. 162. P. 237– 243.

[13] Alenezi M.R., Alzanki T.H.,. Almeshal A.M,. Alshammari A.S., Beliatis M.J., Henley S.J., Silva S.R.P. Hierarchically designed ZnO nanostructure based high performance gas sensors // RSC Adv.. 2014. V. 4. P. 49521–49528.

[14] Zhang Y., Xu J., Xiang Q., Li H., Pan Q., Xu P. Brush-like hierarchical ZnO nanostructures: synthesis, photoluminescence and gas sensor properties // J. Phys. Chem. C. 2009. V. 113. P. 3430–3435.

[15] Migushchenko R.P., Suchkov G.M., Radev Kh.K., Petrishchev O.N., Desyatnichenko A.V. Electromagnetic-acoustic transducer for ultrasonic thickness measurement of ferromagnetic metal products without dielectric coating removal // Technical electrodynamics. 2016. № 2. pp. 78-82.

[16] Lupan O., Cretu V., Postica V., Ahmadi M., Cuenya B.R., Chow L., Tiginyanu I., Viana B., Pauporté T., Adelung R. Silver-doped zinc oxide single nanowire multifunctional nanosensor with a significant enhancement in response // Sensors and Actuators B. 2016. V. 223. P. 893–903.

[17] Rozhansky I.V., Zakgeym D.A. The modeling of polycrystalline ceramic semiconductor electrical properties with submicrometer grain sizes // FTP. 2005. V. 39 (5). pp. 608-615.

[18] Zinc oxide materials for electronic and optoelectronic device applications, ed. by C.W. Litton, D.C.

Reynolds, T.C. Collins. United Kingdom, John Wiley & Sons, Ltd., 2011.

[19] Brillson L.J., Lu Y. ZnO Schottky barriers and ohmic contacts // J. Appl. Phys. 2011. V. 109. P. 121301-1–121301-33.

[20] Mazda F.F. Electronic Instruments and Measurement Techniques. Cambridge, Cambridge University Press, 1987.

[21] Mukae K., Tsuda K., Nagasawa I. Capacitance-vs-voltage characteristics of ZnO varistors // Journal of Applied Physics. 1979, V. 50. P. 4475–4476.

[22] Ramírez M.A., Fernández J.F., Frutos J. Microstructural and nonohmic properties of ZnO.Pr_6O_{11} CoO polycrystalline system // Materials Research. 2010. V. 13. P. 29 – 34.

[23] Morkoç H., Özgür Ü. Zinc Oxide: Fundamentals, Materials and Device Technology. Weinheim, WILEY-VCH Verlag GmbH & Co. KGaA, 2009.